Published in Groundwater Flow and Quality Modelling, 761-775, 1988
(NATO Science Series C : 224)
which should be used for any reference to this work

LARGE SCALE 3-D GROUNDWATER FLOW MODELLING IN HIGHLY HETEROGENEOUS GEOLOGIC MEDIUM.

L. Kiraly
Center of Hydrogeology (University of Neuchâtel)
Rue Emile Argand 11.
CH-2000 Neuchâtel (Switzerland)

ABSTRACT. Regional modelling of groundwater flow in highly heterogeneous geologic medium often requires the simulation of one-dimensional or two-dimensional discontinuities (regional faults, karstic networks, thin aquifers) embedded in an otherwise "continuous" medium. However, finite element models allowing for the association of 1-D, 2-D and 3-D elements are not yet widely used, very probably because of the problems related to the calculation of 2-D element matrixes in a 3-D global space. A simple method, making use of the metric tensor, is proposed to overcome these difficulties and the assebly of 1-D, 2-D and 3-D elements will be illustrated by a theoretical example, as well as by the regional groundwater flow model of Northern Switzerland.

1. INTRODUCTION

In consolidated rocks (sandstones, limestones, crystalline rocks, etc.) discontinuities exist at all scales and their extension varies from a few centimeters (microfractures) to tenth of kilometers (geological fault zones). It seems reasonable to represent these discontinuities as networks of different orders of magnitude which are "embedded" in each other. This "nested model" concept of the geological discontinuities explaines, for example, the well known scale effect on the permeabilities in fractured and karstified limestone aquifers (Kiraly, 1975).

The modelling of this kind of nested structures nearly always requires the combination of the continuum approach with the discret fracture model. At a regional scale, for example, the discret fracture model alone could not be realized at all, because of the tremendous amount of discontinuities (of different orders of magnitude) which ought to be introduced into the model. On the other hand, the equivalent continuum approach alone would not show the effect of the regional fault zones or the regionally developed karstic networks on the groundwater flow systems. So it seems reasonable to model the regional faults or karstic networks by 2-D or 1-D "discret" zones, whereas the volumes between them (which contain only lower order fractures or channels) might be modelled by a 3-D equivalent continuum.

Applied to finite element models, the above approach is equivalent to combine 1-D, 2-D and 3-D elements. In groundwater flow problems, however, the finite element models allowing for the association of 1-D, 2-D and 3-D elements are not yet widely used, very probably because of the problems related to the calculation of the 2-D element matrixes in a 3-D global space. In chapter 2 we present a method proposed by Kiraly (1979), which allows to calculate the element matrixes for curvilinear 2-D finite elements embedded in a 3-D global space. Chapter 3 contains a brief description of the regional groundwater flow model of Northern Switzerland, where 2-D and 3-D elements are associated to simulate the highly heterogeneous geologic structure (for more detail see Kimmeier and alii, 1985).

2. 2-D ELEMENT MATRIXES IN A 3-D GLOBAL SPACE.

2.1. Definition of the Problem.

The principle of the finite element method is supposed to be known. We mention only that constant density groundwater flow is described by the general equation

$$S \frac{\partial h}{\partial t} + \frac{\partial}{\partial x^i}\left(K^{ij} \frac{\partial h}{\partial x^j}\right) + q = 0 \qquad (1)$$

where:

- h = hydraulic potential or head [m]
- S_{ij} = specific storativity [1/m]
- K^{ij} = permeability tensor [m/s]
- q = source term [$m^3/s.m^3$]
- x^i = global coordinates [m]

The above equation may be integrated over each element to give a system of linear equations of the form

$$D_{mn} \frac{\partial h^n}{\partial t} + A_{mn} h^n + Q_m = 0$$

where h^n is the nodal head value and Q_m is the nodal discharge. The matrixes D_{mn} and A_{mn} are defined by

$$D_{mn} = \int_R S N_m N_n \, dR \qquad A_{mn} = \int_R \frac{\partial N_m}{\partial x^i} K^{ij} \frac{\partial N_n}{\partial x^j} \, dR$$

where $N_n(s^k)$ are interpolation functions ("form functions") depending on the local, curvilinear coordinates s^k. At any point given by the local coordinates s^k, the global coordinates and the head values are defined by

$$x^i(s^k) = N_n x^{in} \qquad \text{and} \qquad h(s^k) = N_n h^n$$

with x^{in} = global coordinates of the nodal points. The matrix $\partial N_n/\partial x^i = B_{in}$ is the gradient matrix such that

$$\overrightarrow{\text{grad}} \quad h = B_{in} \quad h^n$$

Our problem is related to the calculation of the gradient matrix B_{in} which cannot be obtained by direct derivation of the interpolation functions N_n with respect to the global coordinates x^i. Standard textbooks propose to use the inverse of the Jacobi matrix to obtain B_{in}:

$$\frac{\partial N_n}{\partial x^i} = \left[\frac{\partial x^i}{\partial s^j}\right]^{-1} \quad \frac{\partial N_n}{\partial s^j} = B_{in} \qquad (2)$$

This method works well when the number of the independent local coordinates s^k is the same as the number of the cartesian global coordinates x^i (for example 3-D elements in a 3-D global space or 2-D elements in a 2-D global space).

When 1-D or 2-D elements are mapped into a 3-D global space, the number of the independent local coordinates will be less than the number of the global coordinates, the Jacobi matrix will not be any more an invertible square matrix and equation 2 cannot be used to calculate the gradient matrix.

2.2. Gradient Matrix for 2-D Element in a 3-D Global Space.

We propose a more general method (Kiraly, 1979, 1985) which may be applied to 1-D, 2-D and 3-D elements mapped in a 3-D global space. This method is based on the well known representation of the gradients in curvilinear coordinates (see for example: Klingbeil, 1966 or Teichmann, 1964), and is illustrated by figure 1. In the curvilinear local system we express the gradient vector (at any point s^k of the element) by the covariant base vectors $\vec{a}_k$ and the contravariant components of the gradient J^k :

$$\overrightarrow{\text{grad}} \quad h = \vec{a}_k \quad J^k \qquad (3)$$

with

$$\vec{a}_k = \frac{\partial \vec{r}}{\partial s^k} = \vec{e}_j \quad \frac{\partial x^j}{\partial s^k} = \vec{e}_j \quad \frac{\partial N_n}{\partial s^k} \quad x^{jn}$$

and

$$J^k = g^{ik} \quad J_i = g^{ik} \quad \frac{\partial h}{\partial s^i} = g^{ik} \quad \frac{\partial N_n}{\partial s^i} \quad h^n$$

The contravariant metric tensor g^{ik} is easily computed by making use of the covariant base vectors $\vec{a}_k$:

$$g^{ik} = \left[g_{ik}\right]^{-1} = \left[\vec{a}_i \cdot \vec{a}_k\right]^{-1}$$

where g_{ik} is the covariant metric tensor, an invertible, symmetric square matrix. Replacing the values of $\vec{a}_k$ and J^k in equation 3, we have:

$$\overrightarrow{grad}\ h = \vec{e}_j \left[\frac{\partial x^j}{\partial s^k}\ g^{ik}\ \frac{\partial N_n}{\partial s^i}\right] h^n = \vec{e}_j\ B^j{}_n\ h^n \qquad (4)$$

The term in brackets is clearly the gradient matrix and $B^j{}_n.h^n$ are the cartesian components of the gradient vector in the global system. The only "extra work" which we have to do with respect to the standard method is the computation of the metric tensors g_{ik} and g^{ik}, but this extra work is largely compensated by the generality thus gained.

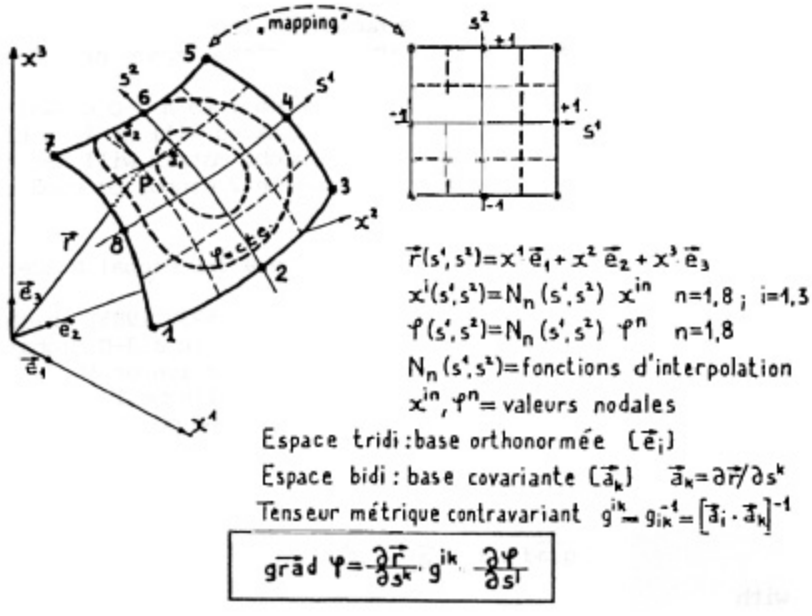

Figure 1. Representation of gradients in curvilinear coordinates

To make the method more "transparent" let us define the gradient matrix for the 8-node element in figure 1. To do this we introduce a more explicit notation for the variables: $s = s^1$, $t = s^2$, $x = x^1$, $y = x^2$, $z = x^3$; $x_1 \ldots x_8$, $y_1 \ldots y_8$, $z_1 \ldots z_8$ are the global coordinates of the nodal points and [B] is the gradient matrix $\partial N_n / \partial x^j$:

$$[B]_{3*8} = \begin{bmatrix} \frac{\partial x}{\partial s} & \frac{\partial x}{\partial t} \\ \frac{\partial y}{\partial s} & \frac{\partial y}{\partial t} \\ \frac{\partial z}{\partial s} & \frac{\partial z}{\partial t} \end{bmatrix} \begin{bmatrix} g_{11} & g_{12} \\ g_{21} & g_{22} \end{bmatrix}^{-1} \begin{bmatrix} \frac{\partial N_1}{\partial s} & \cdots & \frac{\partial N_8}{\partial s} \\ \frac{\partial N_1}{\partial t} & \cdots & \frac{\partial N_8}{\partial t} \end{bmatrix}$$

$$g_{11} = \left(\frac{\partial x}{\partial s}\right)^2 + \left(\frac{\partial y}{\partial s}\right)^2 + \left(\frac{\partial z}{\partial s}\right)^2$$

$$g_{22} = \left(\frac{\partial x}{\partial t}\right)^2 + \left(\frac{\partial y}{\partial t}\right)^2 + \left(\frac{\partial z}{\partial t}\right)^2$$

$$g_{12} = g_{21} = \frac{\partial x}{\partial s} \cdot \frac{\partial x}{\partial t} + \frac{\partial y}{\partial s} \cdot \frac{\partial y}{\partial t} + \frac{\partial z}{\partial s} \cdot \frac{\partial z}{\partial t}$$

and

$$\begin{bmatrix} \frac{\partial x}{\partial s} & \frac{\partial x}{\partial t} \\ \frac{\partial y}{\partial s} & \frac{\partial y}{\partial t} \\ \frac{\partial z}{\partial s} & \frac{\partial z}{\partial t} \end{bmatrix} = \begin{bmatrix} x_1 & \cdots & x_8 \\ y_1 & \cdots & y_8 \\ z_1 & \cdots & z_8 \end{bmatrix} \begin{bmatrix} \frac{\partial N_1}{\partial s} & \frac{\partial N_1}{\partial t} \\ \vdots & \vdots \\ \frac{\partial N_8}{\partial s} & \frac{\partial N_8}{\partial t} \end{bmatrix}$$

As the differential dR is given by $dR = \sqrt{\det g_{ij}}\ .ds\ dt$, we can calculate the 2-D element matrix A_{mn} by numerical integration in the local coordinates

$$A_{mn} = \int_{-1}^{+1}\int_{-1}^{+1} K\ B^j_m\ \ B_{jn}\ \ \sqrt{\det g_{ik}}\ \ ds\ dt \qquad (5)$$

where K is the isotropic permeability in the 2-D element.

Simple numerical examples are given by Kiraly (1979, 1985) and figure 2 shows the calculated results for an oversimplified fractured bloc built up of 1-D, 2-D and 3-D Lagrangian quadratic elements. Laterally and downward the bloc has no-flow boundaries, infiltration is uniformly distributed on the upper surface. The discharge area is concentrated at node 213, where the head is imposed.

The test runs so far executed show a good behaviour of the elements when the number of integration points is reduced to the minimum and the distortion of the elements remains in reasonable limits. Some undesirable properties of the 1-D and 2-D elements will be mentioned in the Conclusions (chapter 4).

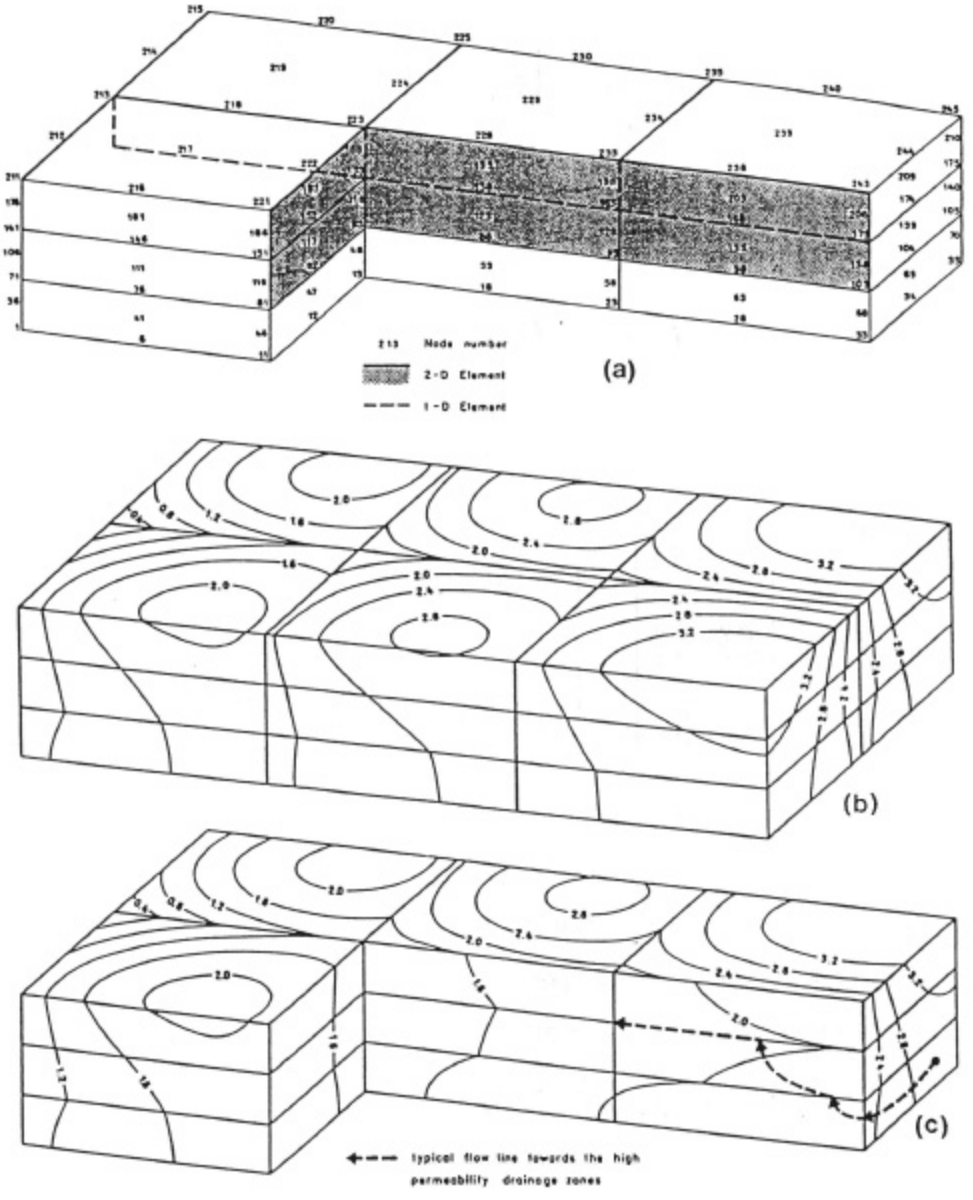

Figure 2. Fractured block model with 1-D, 2-D and 3-D elements (a). - Calculated head distribution is shown by (b) and (c).

3. THE REGIONAL GROUNDWATER FLOW MODEL OF NORTHERN SWITZERLAND.

The regional groundwater flow model of Northern Switzerland has been developed for NAGRA (National Cooperative for the Storage of Radioactive Waste) by the Center of Hydrogeology of the University of Neuchâtel. The principal aim of the model is to simulate the regional groundwater flow systems in the deep crystalline basement for various hypotheses on the boundary conditions and permeability distributions. The structure of the model, as well as the results obtained are described in detail by Kimmeier and alii (1985). The present paper contains only a rather general description, mainly to illustrate the highly heterogeneous geologic medium.

3.1. Geological Setting.

The modelled region extends between two mean areas of crystalline outcrops, the Aar Massive in the south and the Black Forest in the north (figure 3). Between the two massives there are several very different geological and geomorphological units:

- helvetic nappes and flysch in the alpine region
- very thick tertiary sediments in the molasse basin
- limestone synclines and anticlines in the folded Jura
- gently dipping mesozoic series in the tabular Jura
- the Rhine rift valley

These units are shown by the simplified geologic profile of figure 4 and by figure 3. The lithologic series are grouped in a few aquifers and aquitards, explicitly introduced into the model:

- the tertiary flysch and molasse sediments are considered as aquitards.
- the helvetic nappes (mainly mesozoic limestones and marls) are considered globally as an aquifer.
- the autochtonous Malm limestones form a very important aquifer.
- lower Malm, Dogger, Lias and Keuper are grouped to form an important aquitard.
- in the western part of the model a thin limestone aquifer is introduced into the Dogger (the Hauptrogenstein).
- the upper Muschelkalk (in the Triasic) is considered as an important aquifer.
- middle and lower Muschelkalk form a very important, regionally developed aquitard (with gypsum, anhydrite and salt).
- the top crystalline (about 500 m thick) and a thin Buntsandstein layer are put together to form an aquifer.
- beneath, the crystalline is considered as a low permeability rock mass.

3.2. Geometry of the Finite Element Network.

The regional model extends over 23000 km^2, although the mean interest of NAGRA is focused on a much smaller area, simulated by a local model (figure 5 and figure 10). The finite element network is shown by the block-diagram of figure 6, where the lower boundary of the model is

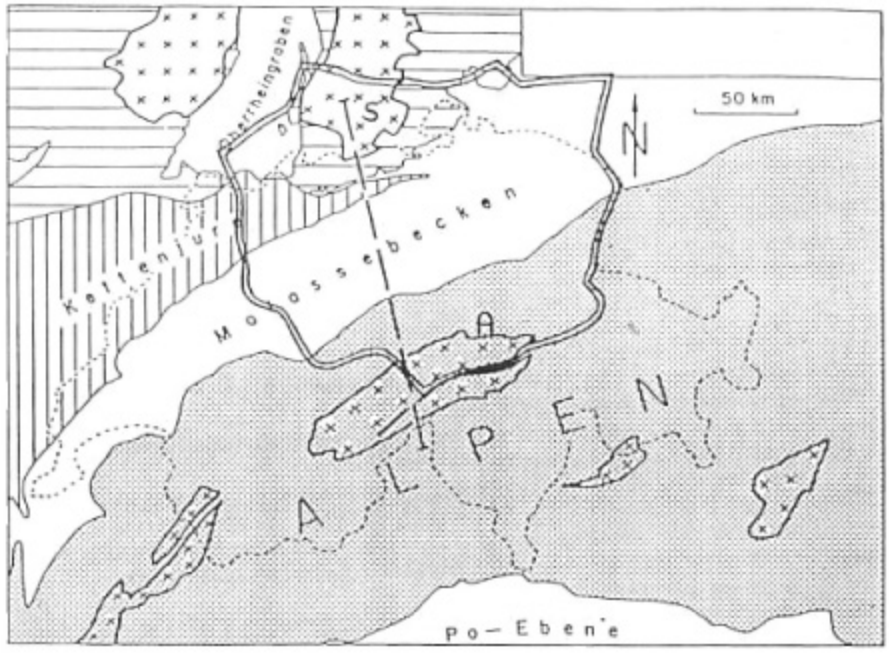

Figure 3. Regional model between Aar Massive (A) and Schwarzwald (S).

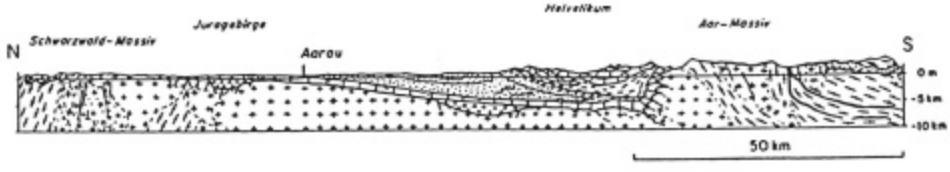

Figure 4. Geologic profile through the model area.

a horizontal plane at a depth of -8000 m. In the regional and the local models we use only quadratic finite elements.

On the upper surface of the model the element sides have a rather "irregular" geometry because they must respect the shape of the geological boundaries and the geometry of the principal valleys representing the mean discharge areas of the groundwater.

Aquitards and thick aquifers are simulated by 3-D element layers, whereas thin aquifers (Hauptrogenstein, Upper Muschelkalk) are simulated by 2-D element "sheets" introduced in sandwich between the aquitards.

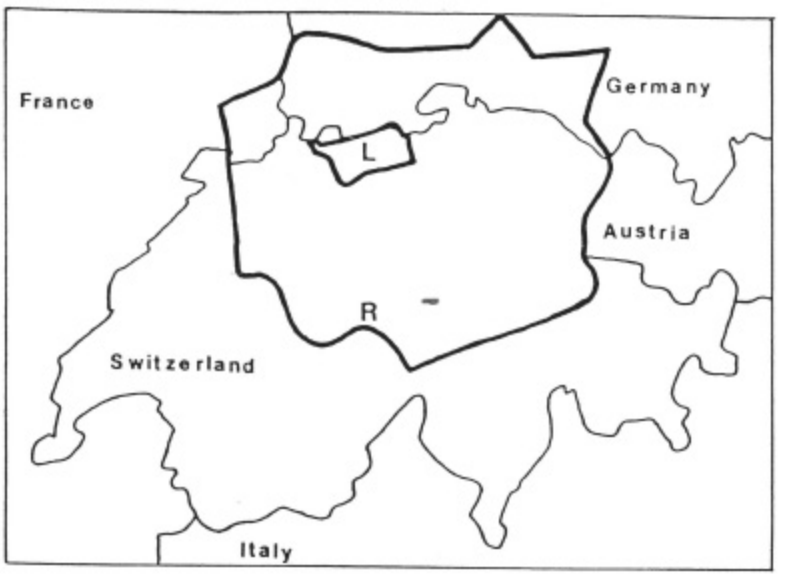

Figure 5. Geographical location of the regional model (R) and the local model (L).

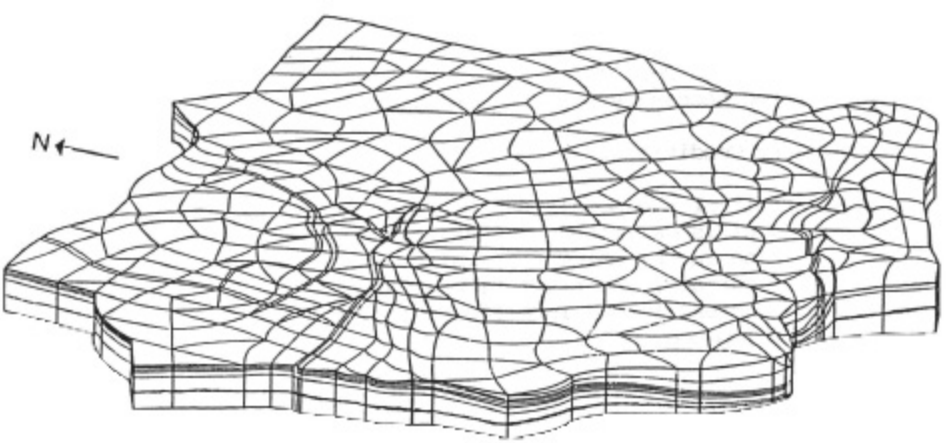

Figure 6. Finite element network of the regional model

Note that Hauptrogenstein and Upper Muschelkalk outcrops are always simulated by 3-D elements. Geologic faults are simulated by 2-D elements according to the methode described in Chapter 2, and figure 7 shows some of the most important regional fault zones introduced into the model.

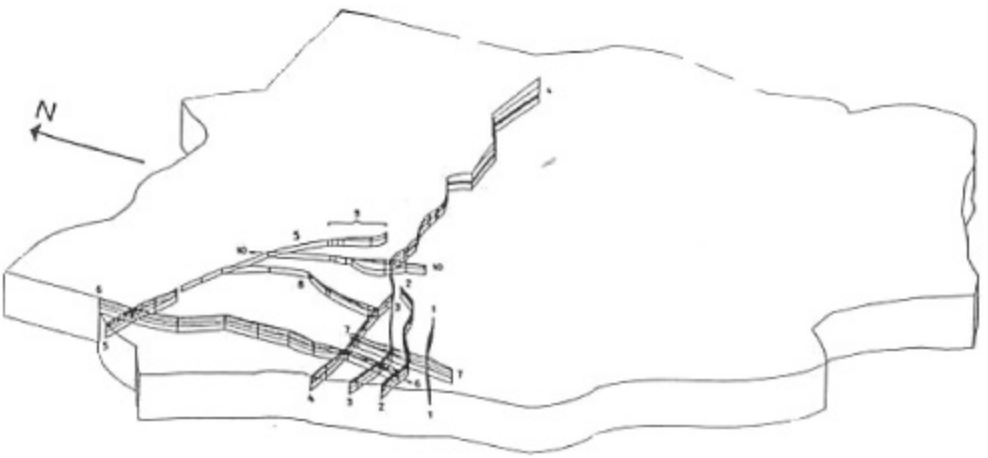

Figure 7. The most important regional fault zones.

The model contains 3635 3-D elements, 1738 2-D elements and 258 1-D elements. There are 14768 nodal points in the regional model. Note that using 1-D and 2-D elements does not increase the number of nodes which would be necessary for the 3-D elements alone.

Boundary Conditions.

The lower limit of the model is a horizontal no-flow boundary. Laterally the model is delimited by vertical no-flow boundaries, excepting a small section in the Rhine rift-valley where the heads are imposed. On the upper surface, the river network always represents fixed head boundaries, whereas in the interfluves infiltration rates or fixed heads may be imposed.

We have to stress out that the form and the size of the regional model is conditioned by the possibility to find "good" lateral no-flow boundaries. In our case, for example, the regional model is much larger than the region of interest defined by NAGRA (see figure 5), because the "good" lateral no-flow boundaries are located far away from the area of detailed investigation. As the groundwater flow must be simulated to great depths even in the local model, we had to seek for "deep" no-flow boundaries. The choosen boundaries represent either major groundwater divides, or major discharge areas where the direction of the groundwater flow should be mainly subvertical. Calculated

Figure 8. Example of fixed head boundary conditions imposed on the upper surface of the regional model.

results of the regional model supply boundary conditions for the finer discretized local model.

3.4. Permeabilities

Scarcity of measured permeability values represented the principal problem in simulating the regional groundwater flow systems. When available, the actual permeability values showed variation over several orders of magnitude, even in the same aquifer or aquitard. For example, the permeability values measured in the crystalline rocks range from 10^{-11} m/s to 10^{-6} m/s. Averaging over large elements, extrapolating the values to regions with no data available or estimating regional anisotropy from the geological structure was necessary for each variant.

As a matter of fact, we used the model as a tool to analyze the sensitivity of the solution to a wide range of hypotheses on the permeability distribution (for more detail see Kimmeier and alii, 1985).

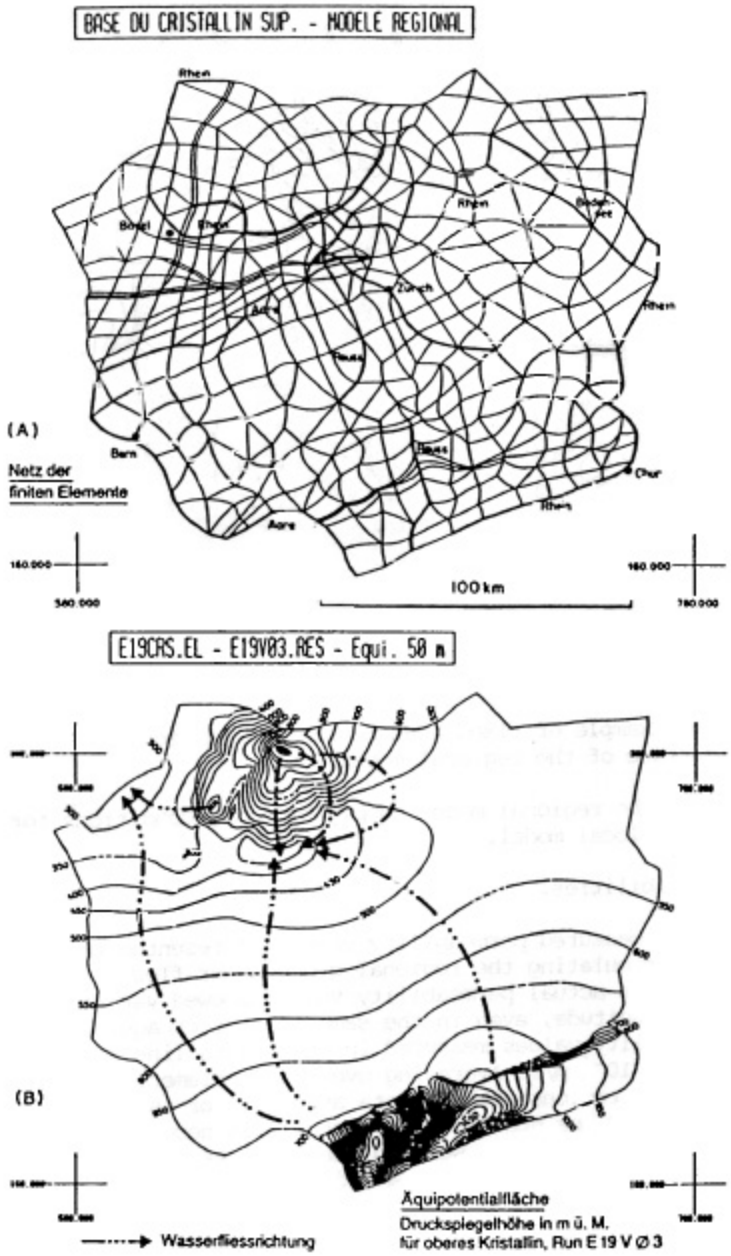

Figure 9. Example of calculated head distribution in the upper Crystalline (regional model).

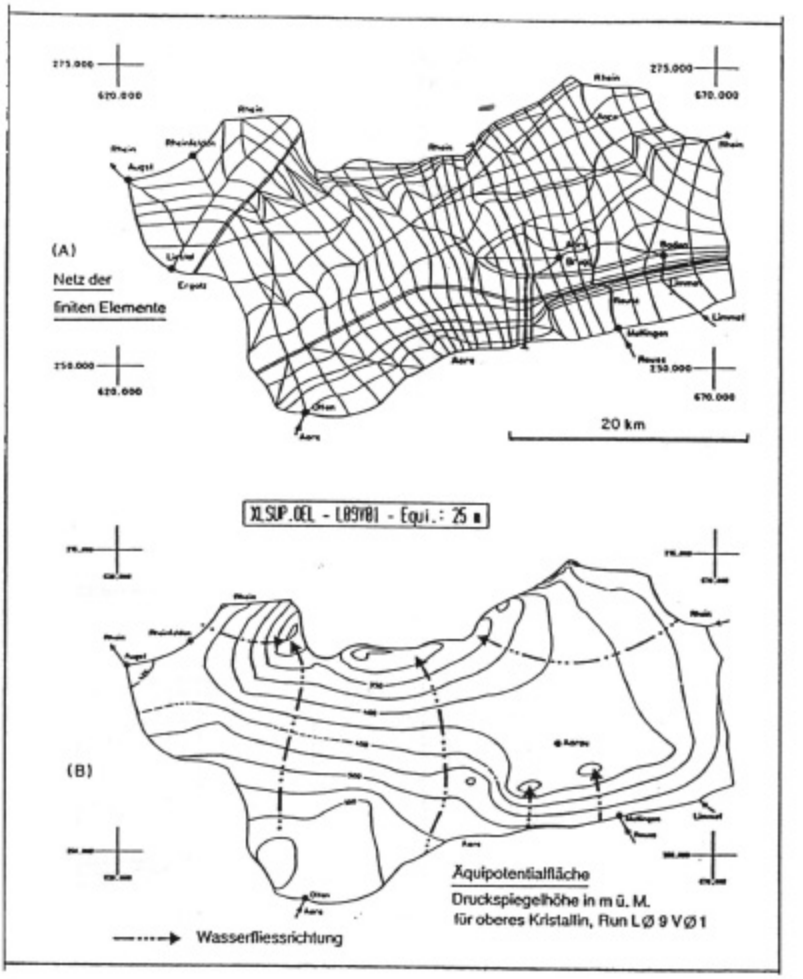

Figure 10. Example of calculated head distribution in the upper Crystalline (local model).

3.5. General Results

If the lack and uncertainity of the data did not allow to obtain a final and unique solution, the regional model as a tool greatly contributed to eliminate a lot of contradictory hypotheses on the boundary conditions and the permeability distribution (for example: too high or too low calculated heads for a given infiltration, or too much infiltration for a given imposed head distribution).

The model has shown that regional flow systems may exist in the crystalline rocks down to great depths. The region of detailed

investigation defined by NAGRA turned out to be located in a regional discharge area (figure 9, 10 and 11). As suggested by figure 11, upward directed hydraulic gradients could exist in the crystalline even at distances of several kilometers from the Rhine. We have to stress out that these upward directed hydraulic gradients were really observed in the deep boreholes completed by NAGRA. The differences between measured and simulated heads in the crystalline rocks range from 10 to 60 m for the best variants.

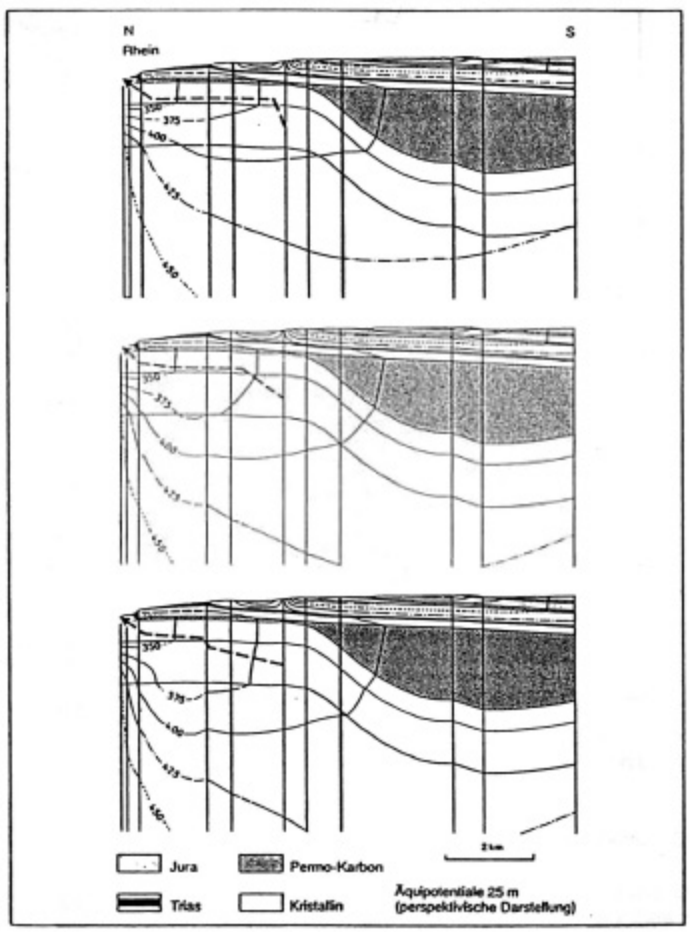

Figure 11. Equipotentials in the vicinity of the Rhine for three hypotheses on the permeability distribution.

4. CONCLUSIONS.

Combining the continuum approach with the "discret fracture" model seems to be a reasonable way to model highly heterogeneous geologic medium at a regional scale. In finite element models, the association of 1-D, 2-D and 3-D elements can be easily completed by using the method described in Chapter 2. As the presence of 1-D or 2-D elements in the model does not increase the number of nodes which would be necessary for the 3-D elements alone, the discontinuities can be put in, or taken out of the model without difficulty.

Associating 1-D, 2-D and 3-D elements has, however, a serious drawback which drives to despair the users of some very fine flow-path calculation routines: the 1-D and 2-D elements "trap" the flow lines. Figure 12 shows that, in fact, a flow line which is well identified in a 3-D element will "lose its identity" when it enters into a 2-D zone, and the point where it leaves the 2-D element is completely undetermined. This is naturally very bad for travel time calculations, but we may ask the question: is the situation illustrated by figure 12 so unrealistic, indeed?

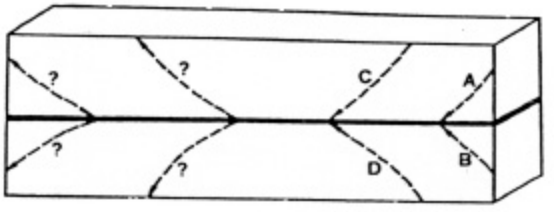

Figure 12. Flow line identification problem in 2-D elements.

REFERENCES:

Kimmeier, F., Perrochet, P., Andrews, R., Kiraly, L., 1985: Simulation des écoulements souterrains entre les Alpes et la Forêt Noire par modèle mathématique. NAGRA NTB 84-50, 169 p.

Kiraly, L., 1975: Rapport sur l'état actuel des connaissances dans le domaine des caractères physiques des roches karstiques. In: Hydrogeology of karstic terrains; éditeurs A.Burger et L. Dubertret, A.I.H., Paris, 53-67.

Kiraly, L., 1979: Remarques sur la simulation des failles et du réseau karstique par éléments finis dans les modèles d'écoulement. Bull. du Centre d'Hydrogéologie Univ. de Neuchâtel, No 3, 155-167.

Kiraly, L., 1985: FEM301 - A three dimensional model for groundwater simulation. NAGRA NTB 84-49, 96 p. + listing.

Klingbeil, E., 1966: Tensorrechnung für Ingenieure. Bibl. Inst. Mannheim, 194 p.

Teichmann, H., 1964: Physikalische Anwendungen der Vektor- und Tensorrechnung. Bibl. Inst. Mannheim, 231 p.